Monthly Notices of the ROYAL ASTRONOMICAL SOCIETY

MNRAS **510,** 6190–6200 (2022) https://doi.org/10.1093/mnras/stab3597
Advance Access publication 2022 January 27

The physics governing the upper truncation mass of the globular cluster mass function

Meghan E. Hughes [1]★ Joel L. Pfeffer [1,2] Nate Bastian,[1,3,4] Marie Martig,[1] J. M. Diederik Kruijssen [5] Robert A. Crain [1] Marta Reina-Campos [6,7] and Sebastian Trujillo-Gomez [5]

[1]*Astrophysics Research Institute, Liverpool John Moores University, 146 Brownlow Hill, Liverpool L3 5RF, UK*
[2]*International Centre for Radio Astronomy Research (ICRAR), M468, University of Western Australia, 35 Stirling Hwy, Crawley, WA 6009, Australia*
[3]*Donostia International Physics Centre (DIPC), Paseo Manuel de Lardizabal 4, 20018 Donostia-San Sebastian, Spain*
[4]*IKERBASQUE, Basque Foundation for Science, E-48013 Bilbao, Spain*
[5]*Astronomisches Rechen-Institut, Zentrum für Astronomie der Universität Heidelberg, Mönchhofstraße 12-14, 69120 Heidelberg, Germany*
[6]*Department of Physics & Astronomy, McMaster University, 1280 Main Street West, Hamilton, L8S 4M1, Canada*
[7]*Canadian Institute for Theoretical Astrophysics (CITA), University of Toronto, 60 St George St, Toronto, M5S 3H8, Canada*

Accepted 2021 November 30. Received 2021 November 10; in original form 2021 April 29

ABSTRACT

The mass function of globular cluster (GC) populations is a fundamental observable that encodes the physical conditions under which these massive stellar clusters formed and evolved. The high-mass end of star cluster mass functions are commonly described using a Schechter function, with an exponential truncation mass $M_{\rm c,*}$. For the GC mass functions in the Virgo galaxy cluster, this truncation mass increases with galaxy mass (M_*). In this paper, we fit Schechter mass functions to the GCs in the most massive galaxy group ($M_{200} = 5.14 \times 10^{13}\,{\rm M}_\odot$) in the E-MOSAICS simulations. The fiducial cluster formation model in E-MOSAICS reproduces the observed trend of $M_{\rm c,*}$ with M_* for the Virgo cluster. We therefore examine the origin of the relation by fitting $M_{\rm c,*}$ as a function of galaxy mass, with and without accounting for mass loss by two-body relaxation, tidal shocks and/or dynamical friction. In the absence of these mass-loss mechanisms, the $M_{\rm c,*}$-M_* relation is flat above $M_* > 10^{10}\,{\rm M}_\odot$. It is therefore the disruption of high-mass GCs in galaxies with $M_* \sim 10^{10}\,{\rm M}_\odot$ that lowers the $M_{\rm c,*}$ in these galaxies. High-mass GCs are able to survive in more massive galaxies, since there are more mergers to facilitate their redistribution to less-dense environments. The $M_{\rm c,*} - M_*$ relation is therefore a consequence of both the formation conditions of massive star clusters and their environmentally dependent disruption mechanisms.

Key words: methods: numerical – globular clusters: general – galaxies: evolution – galaxies: formation – galaxies: star clusters: general.

1 INTRODUCTION

The luminosity, or mass, function of globular clusters (GCs) is one of the most fundamental observables to link the formation of star clusters to 'normal' star formation processes. Unlike the near power-law mass functions of young star clusters (or young 'massive' clusters, YMCs; e.g. Whitmore & Schweizer 1995; Miller et al. 1997; Larsen 2002), generally considered to be the young equivalents of today's old GCs (see reviews by Portegies Zwart, McMillan & Gieles 2010; Kruijssen 2014; Forbes et al. 2018; Krumholz, McKee & Bland-Hawthorn 2019), the luminosity/mass functions of GCs appear peaked at similar magnitudes in all environments, corresponding to a turnover mass of $M_{\rm TO} \approx 2 \times 10^5\,{\rm M}_\odot$ (e.g. Harris 2001; Brodie & Strader 2006; Jordán et al. 2007).

If we take the view that the GCs we observe today formed in a similar way to the YMCs forming in the local Universe then the mass function must have been transformed in some way at the low mass end. To explain this, we have to take into account that the old GCs we observe at $z = 0$ are the surviving population of those initially formed. Therefore a strong possibility to explain the transformation in the mass function is a preferential destruction of low mass star clusters by dynamical processes (e.g. Okazaki & Tosa 1995; Baumgardt 1998; Vesperini 1998; Vesperini et al. 2003; Fall & Zhang 2001; de Grijs, Bastian & Lamers 2003; Goudfrooij 2004; Gieles et al. 2006a; Elmegreen 2010; Kruijssen et al. 2012b).

Traditionally, the GC luminosity/mass function has been modelled as a Gaussian or lognormal distribution to fit the peak (or turnover) of the luminosity function (e.g. Hanes 1977; Harris & Racine 1979; van den Bergh 1985; Harris 2001). The turnover mass (or luminosity) varies only weakly with galaxy mass (Jordán et al. 2007; Villegas et al. 2010). The high mass end of the GC mass function (i.e. above the turnover mass) has also been shown to be well fit by a power-law function with an index around −1.7 to −2 (Surdin 1979; Racine 1980; Harris & Pudritz 1994; Durrell et al. 1996; Kissler-Patig, Richtler & Hilker 1996), surprisingly close to that observed for YMCs (≈−2 with some galaxy-to-galaxy variations, Whitmore & Schweizer 1995; Miller et al. 1997; Larsen 2002; Zhang & Fall 1999; Bik et al. 2003; McCrady & Graham 2007; Chandar et al. 2010; Whitmore et al. 2014; Messa et al. 2018a).

★ E-mail: M.Hughes1@2013.ljmu.ac.uk

However, at the very high mass end there is evidence for a further steepening of the cluster mass function, for both GCs (Harris & Pudritz 1994; Burkert & Smith 2000) and YMCs (Whitmore et al. 1999; Larsen 2002, 2009; Gieles et al. 2006b; Bastian et al. 2012; Adamo et al. 2015, 2017, 2020; Johnson et al. 2017; Messa et al. 2018a). This steepening, or 'truncation', is generally fit by a Schechter (1976) function, i.e. a power law with an exponential truncation ($M_{c,*}$). For GC mass functions this may be modified in the form of an 'evolved' Schechter function in order to fit both the high-mass truncation and turnover at lower masses (Jordán et al. 2007). In the case of YMCs, the truncation may vary with local environment (namely the star formation rate surface density, Portegies Zwart et al. 2010; Adamo et al. 2015, 2020; Johnson et al. 2017; Messa et al. 2018b; though see Mok, Chandar & Fall 2019 for evidence for a constant truncation mass). Reina-Campos & Kruijssen (2017) predict that the high mass end of the GC mass function does not depend on the absolute star formation rate, but instead is set by a combination of galactic dynamics and stellar feedback, resulting in an effective scaling with the gas and star formation rate surface densities. It is only when accounting for the interplay between both mechanisms that they can reproduce the observed trends of $M_{c,*}$ with galactocentric radius.

In the case of GCs, fewer studies have investigated systematic trends of the upper truncation with galaxy properties. Jordán et al. (2007) analysed the luminosity and mass function of evolved GCs observed by the ACS Virgo Cluster Survey to investigate the dependence of the GC luminosity and mass function on galaxy stellar mass. They find that the luminosity function of the GCs shows a decreasing $M_{c,*}$ value with decreasing galaxy mass. They argue that the behaviour at the high mass end of the GC mass function is a consequence of systematic variations of the initial cluster mass function rather than long-term dynamical evolution.

In this work, we compare the relation between $M_{c,*}$ and galaxy mass in the E-MOSAICS simulations (Pfeffer et al. 2018; Kruijssen et al. 2019a; Crain et al. in prep.) to that found by Jordán et al. (2007). The E-MOSAICS simulations trace the formation and evolution of GC populations alongside galaxy formation and evolution, and therefore enable us to investigate the impact of various galaxy properties on the resulting GC observables. Specifically for this work, we can explore how GC formation environment and GC mass loss play a role in initializing and evolving the GC mass function. The E-MOSAICS simulations have been shown to reproduce and provide an explanation for a range of observed properties of both young and old GCs, such as the existence of a 'blue tilt' in GC populations (Usher et al. 2018), as well as the fraction of disrupted GC stars in the bulge (Hughes et al. 2020) and the halo (Reina-Campos et al. 2018, 2020) of the Milky Way. The simulations have shown that the diversity in age–metallicity relations of Milky Way-mass galaxies results from different assembly histories and can therefore be used to infer such assembly histories (Kruijssen et al. 2019a, b, 2020). The simulations have also been shown to reproduce the observed kinematics of the Galactic GC population (Trujillo-Gomez et al. 2021) and have been used to conclude that GCs associated with stellar streams will be, on average, younger than the GC population not associated with a stellar stream (Hughes et al. 2019), a result subsequently confirmed through observations of stellar streams in the halo of M31 (Mackey et al. 2019). Finally, Pfeffer et al. (2019) showed that the simulations reproduce the properties of young cluster populations, and the simulations were subsequently used to predict when and where GCs formed (Reina-Campos et al. 2019; Keller et al. 2020). By comparing the simulation outputs to the observations of Jordán et al. (2007), this work will serve as another test that YMCs and ancient GCs share the same formation mechanism. However, previous work showed the E-MOSAICS simulations do not reproduce the observed GC turnover mass, most likely due to under-disruption of low-mass GCs in the simulations (see Pfeffer et al. 2018; Kruijssen et al. 2019a). Therefore in this work, we focus on the high-mass end of the GC mass function (i.e. the exponential truncation $M_{c,*}$).

This paper is organized as follows. In Section 2, we outline the aspects of the E-MOSAICS simulations important for this work. In Section 3, we describe the observational data and compare them to the simulations. In this section, we also justify our choice to fit Schechter (1976) functions instead of a single power-law function. Section 4 investigates the impact of considering alternative cluster formation scenarios on the mass functions. Section 5 describes how the mass function changes when including the initial masses of GCs that have been completely disrupted. Finally, in Section 6 we present our conclusions.

2 SIMULATIONS

The E-MOSAICS suite of simulations (Pfeffer et al. 2018; Kruijssen et al. 2019a) couples the MOSAICS (Kruijssen et al. 2011; Pfeffer et al. 2018) model for star cluster formation and evolution to the EAGLE (Schaye et al. 2015; Crain et al. 2015) model for galaxy formation. This enables the simulations to follow simultaneously the formation and evolution of star clusters and their parent galaxies in a cosmological context. This work uses the E-MOSAICS 34.4^3 comoving Mpc^3 periodic volume (Crain et al. in prep.), first featured in Bastian et al. (2020). The E-MOSAICS model is the same as described for the E-MOSAICS zoom-in simulations (Pfeffer et al. 2018; Kruijssen et al. 2019a). The simulations have gas particles with initial masses $m_g = 2.25 \times 10^5\,\mathrm{M}_\odot$.

EAGLE is a set of hydrodynamical simulations of the formation of a cosmologically representative sample of galaxies in a ΛCDM cosmogony, meaning that a wide range of galaxy environments are sampled. The simulations include sub-grid radiative cooling (Wiersma et al. 2009), star formation (Schaye & Dalla Vecchia 2008), stellar feedback (Dalla Vecchia & Schaye 2012), chemical evolution (Wiersma et al. 2009), gas accretion on to, and mergers of, super massive black holes (BHs) (Rosas-Guevara et al. 2015) and active galactic nuclei (AGN) feedback (Booth & Schaye 2009). The standard resolution EAGLE simulations yield a galaxy stellar mass function that reproduces the observed function to within 0.2 dex over the well-sampled and well-resolved mass range. For a full description of the models, see Schaye et al. (2015).

The EAGLE model has been shown to reproduce many important galaxy properties, such as galaxy masses, sizes, luminosities and colours (Furlong et al. 2015, 2017; Trayford et al. 2015), as well as their cold gas properties (e.g. Lagos et al. 2015; Crain et al. 2017) and cosmic star formation rate density (Furlong et al. 2015). The wide range of reproduced galaxy properties across a wide range of galaxy masses makes the EAGLE model ideal for comparing with observed galaxy properties.

The MOSAICS model adds a subgrid component of star cluster formation and evolution into the EAGLE simulations. When a stellar particle forms in the simulations it has the ability to convert some of its (subgrid) mass into a star cluster population. The star clusters then acquire the position, velocity, age and chemistry of their host stellar particle. The fraction of mass assigned for star cluster formation in a stellar particle is determined by the cluster formation efficiency (CFE) and is dependent on the local natal gas pressure (Kruijssen 2012). Once the fraction of mass has been assigned, cluster masses

are stochastically drawn from a Schechter (1976) mass function with an exponential truncation mass $M_{c,*}$ that is environmentally dependent (Reina-Campos & Kruijssen 2017),

$$dN/dM \propto M^{\alpha} \exp(-M/M_{c,*}), \quad (1)$$

where α is the index of the power law part of the function for masses below the truncation mass $M_{c,*}$, above which the function can be described by an exponential. Observations of YMC populations indicate that $\alpha \simeq -2$ (e.g. Zhang & Fall 1999; McCrady & Graham 2007; Dowell, Buckalew & Tan 2008; Baumgardt et al. 2013; Adamo & Bastian 2018). The giant molecular cloud mass function has a similar, but slightly shallower slope (see Chevance et al. 2020 for a recent review). This power-law index has been used to describe the distributions of masses of many stellar systems within a galaxy and is likely the result of fragmentation produced by the balance between gravitational collapse and turbulence compression (Elmegreen 2011; Adamo et al. 2020).

The Reina-Campos & Kruijssen (2017) model assumes that $M_{c,*}$ is proportional to the mass of the most massive molecular cloud (Kruijssen 2014). The model predicts that the largest cloud mass is set by the interplay between the gravitational collapse of the largest unstable region in a differentially-rotating disk, i.e. the Toomre (1964) mass, and stellar feedback from the newborn stellar population within that region. If stellar feedback halts and disperses the collapsing region, the resulting cloud mass is smaller than the Toomre (1964) mass. This model predicts that, in the feedback-limited regime, $M_{c,*}$ increases in environments with higher gas pressures, as feedback becomes less efficient in such environments.

Star clusters lose mass in the simulations through stellar evolution and dynamical processes. Stellar mass-loss follows the EAGLE model (Wiersma et al. 2009). Dynamical mass-loss is due to two-body relaxation, tidal shocks and total disruption through dynamical friction. The contributions from two-body relaxation and tidal shocks are calculated via the local tidal tensor and dynamical friction is applied at every snapshot in post-processing. The dynamical friction timescale is calculated for all clusters at each simulation snapshot and clusters can be completely removed by dynamical friction when the dynamical friction timescale is less than the age of the cluster (see Pfeffer et al. 2018, for full details).

Pfeffer et al. (2019) compare the $M_{c,*}$ of young star cluster populations in the E-MOSAICS simulations with observations of local galaxies and find good agreement, though more observations of systems with young star clusters are needed to test whether the scatter found in the simulations is realistic. In this work, we expand on the Pfeffer et al. (2019) study to contrast the $z = 0$ $M_{c,*}$ of GC systems (with no age constraints) to that of observations. This means that we allow the E-MOSAICS initial cluster mass function to evolve with time (through stellar evolution and dynamical processes) and test whether observations are still matched. This is a test of the cluster formation physics in the simulations and also the subsequent evolution of the star clusters alongside their host galaxies.

3 COMPARISON BETWEEN SIMULATIONS AND OBSERVATIONS

3.1 Virgo Cluster Data

The data we compare our simulations to throughout this work are part of the ACS Virgo Cluster Survey, first presented by Côté et al. (2004). The survey is designed to observe 100 early-type galaxies in the Virgo Cluster, using the Advanced Camera for Surveys (ACS) on the *Hubble Space Telescope*. The survey used the F475W and the F850LP bandpasses (approximately equal to the Sloan g and z respectively, Côté et al. 2004). The ACS Virgo Cluster Survey is designed to probe the brightest ≈ 90 per cent of the GC luminosity function in the 100 galaxies. This yields a sample of ≈13 000 GCs in the Virgo Cluster (Côté et al. 2004).

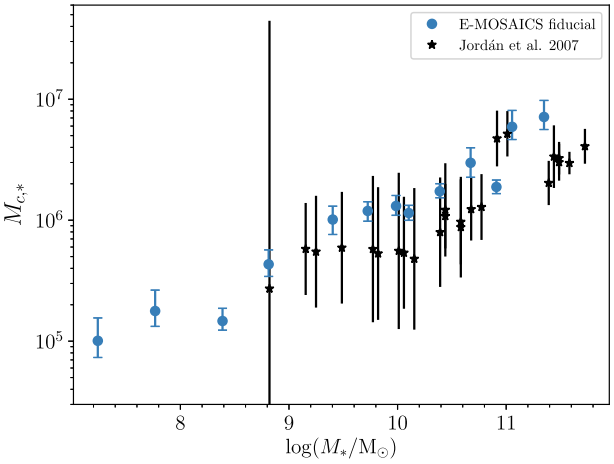

Figure 1. The dependence of $M_{c,*}$ on galaxy stellar mass in the Virgo galaxy cluster and the most-massive E-MOSAICS galaxy group. The black stars represent the data taken from Fig. 16 of Jordán et al. (2007). The blue points show the fits to the E-MOSAICS fiducial model at z = 0, where the error bar represents the 16th–84th percentile range of the posterior distribution. The blue E-MOSAICS points match well with the Jordán et al. (2007) sample.

Jordán et al. (2007) present the luminosities of GCs belonging to early-type galaxies in the ACS Virgo Cluster Survey. They fit the luminosity functions with an evolved Schechter function (which is meant to account for the GC mass loss) and present the truncation luminosity in their table 3, and the corresponding truncation mass ($M_{c,*}$) as a function of galaxy stellar mass based on the B-band galaxy magnitude in their Fig. 16.

Peng et al. (2008) present the stellar masses of the galaxies in the ACS Virgo Cluster Survey. We use their table 1 to obtain the stellar mass for each of the galaxies in the Jordán et al. (2007) sample. The Jordán et al. (2007) results in this format are presented as black stars in Fig. 1.

3.2 Simulation Data

To compare the mass functions of GCs in the E-MOSAICS simulations with those in the Virgo galaxy cluster (Jordán et al. 2007), we use the most massive galaxy group in the simulation, which has a virial mass $M_{200} = 5.14 \times 10^{13}\,\mathrm{M}_\odot$.[1] The stellar mass of the brightest cluster galaxy (BCG) is $M_* = 2.23 \times 10^{11}\,\mathrm{M}_\odot$ and the cluster contains 154 galaxies with a stellar mass above $10^7\,\mathrm{M}_\odot$. The virial mass of the Virgo galaxy cluster has been estimated to be $6.3 \times 10^{14}\,\mathrm{M}_\odot$ by Kashibadze, Karachentsev & Karachentseva (2020) and $4.2 \times 10^{14}\,\mathrm{M}_\odot$ by McLaughlin (1999). This places our simulated galaxy cluster at a lower mass than the Virgo galaxy cluster but similar to the Fornax cluster (Drinkwater, Gregg & Colless 2001). Villegas et al. (2010) showed that the GC mass function dispersion and turnover mass is similar in both the Virgo and Fornax clusters, while Liu et al. (2019) showed the behaviour of specific frequency with galaxy luminosity is also similar. Therefore we consider the

[1]The total mass contained within the radius at which the density drops to 200 times the critical density.

Table 1. The number of galaxies and GCs in each galaxy mass bin and GC sub-population. The highest galaxy mass bins contain just one galaxy, so in this case we give the galaxy's mass.

$\log(M_*/\mathrm{M}_\odot)$	Galaxies	Min. GC mass [$\mathrm{M}_\odot$]	Fiducial	No DF	Initial
7–7.5	41	1.63×10^3	441	476	2609
7.5–8	39	2.66×10^3	884	913	6236
8–8.5	18	3.24×10^3	1184	1211	10690
8.5–9	15	6.67×10^3	1877	1898	17958
9–9.5	10	1.60×10^4	1901	1923	14642
9.5–9.75	6	2.70×10^4	2494	2522	16624
9.75–10	4	5.45×10^4	1301	1844	21364
10–10.25	7	5.68×10^4	2465	3137	55148
10.25–10.5	2	4.21×10^4	1484	1618	33617
10.67	1	5.33×10^4	612	719	36666
10.91	1	7.16×10^4	1323	1548	47650
11.05	1	1.18×10^5	1410	1801	45898
11.35	1	1.14×10^5	2992	3332	42234

comparison of GCs in simulated Fornax-mass clusters with the Virgo cluster to be reasonable. We also show in Section 3.3 that halo mass does not have a strong impact on our results.

3.2.1 *Description of the Schechter function fits*

To fit Schechter functions to the GC mass functions from the simulations, we follow the methodology outlined by Pfeffer et al. (2019), who adopt similar analyses to those used in observational studies (e.g. Johnson et al. 2017; Messa et al. 2018a). We stack all the GCs in the simulated cluster in bins of host galaxy stellar mass and use the Markov Chain Monte Carlo (MCMC) code PyMC (Fonnesbeck et al. 2015) to perform the fits and to sample the posterior distribution of the Schechter power-law index and truncation mass. Stacking galaxies is necessary to increase GC numbers for robust Schechter fits. Jordán et al. (2007) also stack galaxies in the lower-mass galaxy mass bins. The power-law index is sampled with a uniform prior between -3 and -0.5. The truncation mass is sampled in log-space with a uniform prior between a minimum cluster mass (which we describe below) and $10^9\,\mathrm{M}_\odot$. We use a Gaussian likelihood for $\log M_{\mathrm{c},*}$. For each fit the MCMC takes 10 000 steps and we take the first 1000 of these steps as burn-in.

In the galaxy mass range of the Jordán et al. (2007) observations ($\log M_*/M_\odot > 9.5$) we bin the galaxies by stellar mass in bins of width 0.25 dex. Below this mass, we use galaxy stellar mass bins of width 0.5 dex to yield the best sampling. We present the number of galaxies and number of GCs used in Table 1, where the 'fiducial', 'No dynamical friction (DF)' and 'initial' columns refer to three GC subsamples from the simulations that are described in Section 5. In the range of the observations ($\log M_*/M_\odot > 9.5$) the simulated sample contains a similar number of galaxies as the Jordán et al. (2007) study, who also include just 1 galaxy in their most massive bin and 10 in their least massive. We do, however include more GCs in each bin than Jordán et al. (2007): their sample spans a range of 193-1721 GCs, whereas our fiducial sample of GCs spans a number range of 612-2992 within the same galaxy mass range. Due to the lack of a cold, dense gas phase in the EAGLE model, it is a known problem that E-MOSAICS does not disrupt enough low-mass GCs (see Pfeffer et al. 2018; Kruijssen et al. 2019a). Since the $M_{\mathrm{c},*}$ relies on a fit to the high-mass end of the GC mass function this should not affect our $M_{\mathrm{c},*}$ results, but could have an impact on the reliability of the fit to the slope. Indeed, for this reason, we do not attempt to fit turnover masses to the mass functions.

We use a varying minimum cluster mass across the galaxy mass range, in order to restrict the fits to the high-mass end of the GC mass functions (however in Appendix A we consider the effect of different minimum masses for the fits). We therefore fit Schechter functions to the upper 2 dex of the mass function, from the third most massive GC to account for stochasticity at the high-mass end. We find this range sufficient to enable fitting of both the upper truncation ($M_{\mathrm{c},*}$) and power-law index (α). We quote the minimum masses of the GCs in Table 1. The minimum mass adopted also scales with galaxy mass in a similar way to the completeness limit for Virgo GCs. For example, from table 1 in Jordán et al. (2007), Virgo galaxies with stellar masses $M_* \approx 10^9\,\mathrm{M}_\odot$ have a GC completeness of 90 per cent at the luminosity limit $m_z = 25.2$, corresponding to a GC mass of $\approx 2 \times 10^4\,\mathrm{M}_\odot$. Virgo galaxies with mass $M_* \approx 10^{11}\,\mathrm{M}_\odot$ reach GC completeness of 90 per cent at $m_z \approx 23$, corresponding to a GC mass of $\approx 1.5 \times 10^5\,\mathrm{M}_\odot$. Both values are similar to the minimum masses we adopt. We note that the lower galaxy mass bins, outside of the galaxy mass range of the Jordán et al. (2007) observations, include GCs that would be too faint to observe at the distance of the Virgo cluster, but it is still interesting from a theoretical stand point to investigate the continuation of the trend at lower galaxy stellar masses.

3.2.2 *Should we fit upper truncations?*

There is some contention in the literature as to whether Schechter functions or single power laws fit star cluster mass functions more accurately (Chandar et al. 2014, 2016; Mok et al. 2019). Although on a per-particle basis the mass function assumed by the E-MOSAICS fiducial model is a Schechter function with an environmentally dependent $M_{\mathrm{c},*}$, this does not necessarily mean that the final mass function will be best fit by a Schechter function. The GC mass function of each simulated galaxy is an accumulation of the GC populations associated with many particles; each with varying input $M_{\mathrm{c},*}$, and dynamical evolution may erase the signal of any exponential truncation.

Therefore, we also fit power law functions to the GCs in each galaxy mass bin, over the same mass range and with the same MCMC method as described for the Schechter fits above. The power law index is sampled with a uniform prior between -3 and -0.5. We then calculate the Bayesian Information Criterion (BIC) value (Schwarz 1978) for both of the fitting functions and compare them.

The BIC value takes into account that a model with more free parameters is likely to fit the data better and penalises the maximum likelihood estimate of the model if there are more free parameters in the fit. The BIC value is given by,

$$\mathrm{BIC} = k \ln(n) - 2 \ln(L) \tag{2}$$

where k is the number of free parameters in the fit, n is the sample size, L is the maximum likelihood estimate of the model and lower BIC values are favourable. We can compare two models by calculating the difference in their BIC values (ΔBIC). When we subtract the BIC value of the Schechter fit from that of the power law fit, positive values indicate that the Schechter function is preferred over the power law and vice versa. We find that, for all galaxy mass bins, a Schechter function is strongly preferred with Δ BIC values between 18 and 133. In Section 5, we include two more subsamples of GCs which omit specific mass loss mechanisms. A Schechter function is also preferred over a power law function for all galaxy masses in these subsamples. For the subsample of GCs with dynamical friction omitted, Δ BIC values are between $12 - 105$, and for the subsample of GCs with

all mass loss omitted, Δ BIC values are between 2 − 129. Given that all Δ BIC values are positive we are confident that the simulated globular cluster mass functions are better fit by a function with an upper truncation mass.

We compare the effect of varying minimum masses and also the results from the pure power-law fit in Appendix A.

3.3 Truncation masses in simulations versus observations

In Fig. 1, we show $M_{c,*}$ as a function of galaxy stellar mass for the observations from Jordán et al. (2007) and for the most massive galaxy group in the E-MOSAICS simulations. Error bars show the 16th and 84th percentiles of the posterior distribution. Fig. 1 shows good agreement between the truncation masses of the observations and the E-MOSAICS simulations, particularly in the slope of the relation. There is a systematic offset between the two distributions in Fig. 1: $M_{c,*}$ is consistently higher in E-MOSAICS than in the observations. This offset is smaller than the observational uncertainties, but could be due to a number of effects. On the simulation side, under-disruption could mean that $M_{c,*}$ is overestimated (see Appendix D of Kruijssen et al. 2019a), the dynamical friction timescales (calculated in post-processing) could be too long, or the initial $M_{c,*}$ slightly too large. Alternatively, some of the difference may be due to uncertainties in colour-M/L conversions for observed GCs.

In Fig. 2, we show the same observational data from Jordán et al. (2007) as in Fig. 1 but we now show $M_{c,*}$ as a function of galaxy mass for all galaxies in the E-MOSAICS volume, divided by whether they are quiescent or star forming and their group mass. Upward arrows represent the galaxy mass bins where a robust Schechter fit could not be acheived. We define 'field galaxies', 'super L∗ galaxies' and 'cluster galaxies' as having total group masses $M_{200} < 10^{12}$, $10^{12} < M_{200}/\mathrm{M}_\odot < 10^{13}$ and $M_{200} > 10^{13}\,\mathrm{M}_\odot$ respectively. Following the Pfeffer et al. (2019) method, we select galaxies that are currently not on the star forming main sequence based on the specific star formation rate (sSFR) within a 30 kpc aperture. The reasoning for splitting galaxies by their current star formation is two-fold: firstly, galaxies that reside in galaxy clusters (such as those used in Jordán et al. 2007) are likely to be quiescent and secondly, galaxies that are forming massive GCs at $z = 0$ could bias the $M_{c,*}$ fits to high values. Fig. 2 shows that quiescent galaxies in the full E-MOSAICS volume also show agreement in the truncation masses with the Jordán et al. (2007) observed values, whereas those that are star forming have, on average, slightly higher $M_{c,*}$ (possibly due to having slightly younger, less evolved GCs). In the star forming group, some galaxy mass bins could not get a Schechter fit, likely due to greater stochasticity of high-mass GCs. This confirms that there is nothing special about the galaxies in the most massive galaxy group, except that they are likely to be quiescent. Therefore, we continue the rest of this work with the most massive galaxy group to ease comparison with observations and to simplify discussion.

Note that in the model, the $M_{c,*}$ is calculated separately to the power-law index. Therefore, if the power-law index was shallower/steeper, there would be more/fewer GCs at higher masses and although $M_{c,*}$ would be better/worse sampled, its value would remain the same.

Given the above discussion it is still fair to suggest that the E-MOSAICS simulations show mass function truncations that are a satisfactory match to the Jordán et al. (2007) observations and make the clear prediction that $M_{c,*}$ increases with galaxy mass. This demonstrates that the fiducial input physics of the MOSAICS model is able to reproduce a fundamental observable in GC studies.

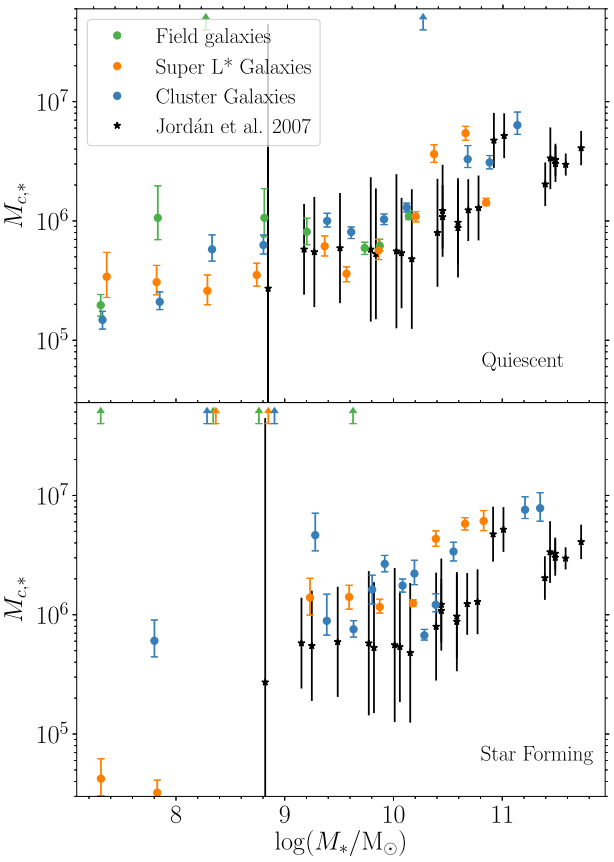

Figure 2. The dependence of $M_{c,*}$ on galaxy stellar mass in the Virgo galaxy cluster and the most-massive E-MOSAICS galaxy group. The black stars represent the data taken from Fig. 16 of Jordán et al. (2007). The coloured points show the fits to the E-MOSAICS volume, split by the group mass 'field': $M_{200} < 10^{12}\,\mathrm{M}_\odot$; 'super L*': $10^{12} < M_{200}/\mathrm{M}_\odot < 10^{13}$; cluster: $M_{200} > 10^{13}\,\mathrm{M}_\odot$). The top panel shows the quiescent galaxies and the bottom panel shows star forming galaxies.

To determine which physical mechanism is the most important in setting the relation in Fig. 1, we will examine alternative formation physics in the next section.

4 ALTERNATIVE CLUSTER FORMATION PHYSICS

In this section, we investigate three alternative cluster formation physics variants in the E-MOSAICS model to establish which of the key ingredients of the model are needed to reproduce the observations of Jordán et al. (2007). We outline the differences between the models below:

(i) In the fiducial model, both the cluster formation efficiency and $M_{c,*}$ depend on environment (as described in Section 2)

(ii) In the 'no formation physics' model, there is a constant cluster formation efficiency ($\Gamma = 0.1$) and no upper truncation to the mass function i.e. it is a pure power law, therefore the cluster formation is not environmentally dependent and is equivalent to a simple 'particle tagging' method.

(iii) In the CFE only model, the CFE varies with environment but there is no upper truncation to the mass function.

(iv) In the $M_{c,*}$ only model, the CFE is a constant ($\Gamma = 0.1$) but $M_{c,*}$ varies with environment.

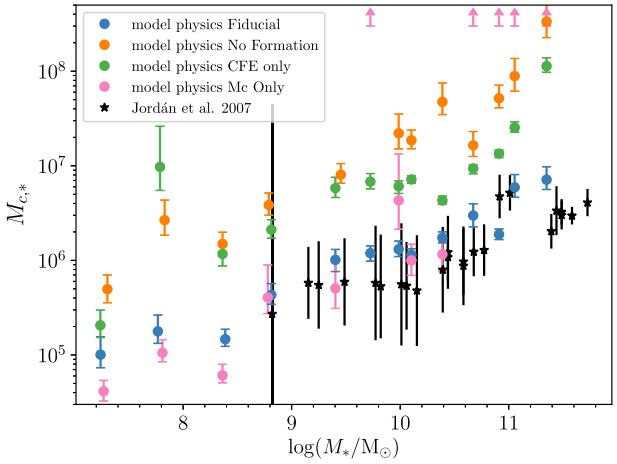

Figure 3. The dependence of $M_{c,*}$ on galaxy stellar mass in the Virgo galaxy cluster and the most-massive E-MOSAICS galaxy group. The fiducial model, the 'no formation' model, the 'CFE only' model and the 'Mc only' model are represented by blue, orange, green and pink circles, respectively.

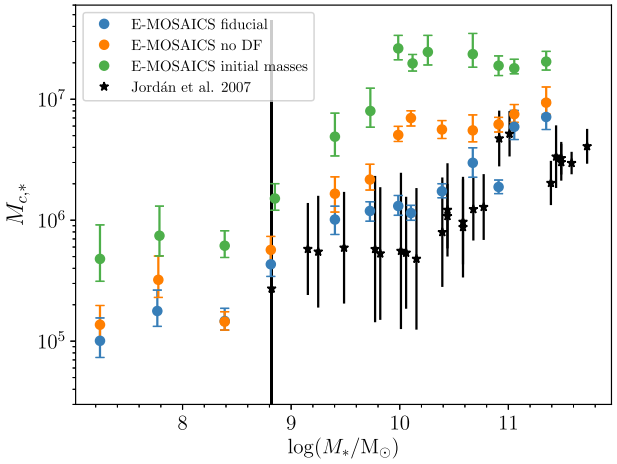

Figure 4. The dependence of $M_{c,*}$ on galaxy stellar mass in the Virgo galaxy cluster and the E-MOSAICS galaxy cluster. The black stars represent the data taken from Fig. 16 of Jordán et al. (2007). The blue points show the E-MOSAICS fiducial model at z = 0. The orange points show the E-MOSAICS model with no dynamical friction taken into account. Finally, the green points show the E-MOSAICS with no mass loss (stellar evolution or dynamical) taken into account. All dynamical evolution processes must be included in the simulation to match well with the Jordán et al. (2007) sample.

In Fig. 3, we present the four alternative physics models in blue, orange, green and pink, respectively. Firstly, we will focus on the 'no formation physics' model (orange), where the increasing trend of $M_{c,*}$ with galaxy stellar mass is simply a size-of-sample effect. More massive galaxies form more GCs and therefore have the potential to sample more massive GCs from the power-law mass function. Dynamical friction then acts to remove some of the most massive GCs and a truncation is detected. The slope of the relation will be constant, but the relation could be shifted up or down, depending on the CFE. However, the slope of the 'no formation physics' model is significantly steeper than that of the observations, with slopes of 0.58 and 0.40, respectively, so even with a smaller CFE to shift the relation to lower $M_{c,*}$, it would not match the observations.

Next, we concentrate on the 'CFE only' model, where the increasing trend of $M_{c,*}$ with galaxy stellar mass is still present and mostly follows that of the 'no formation model', except for a dip in $M_{c,*}$ at $\log(M_*/M_\odot) \approx 10$. The dip occurs because there is now an environmentally dependent CFE so galaxies forming most of their GCs in high pressure regions have the potential to form their most massive GCs here as well, in an environment that can subsequently disrupt them. Therefore it is likely that dynamical evolution is the cause of this slight decrease in $M_{c,*}$, which we discuss further in the context of the fiducial model in Section 5.

Finally, we turn our attention to the '$M_{c,*}$ only' model, here we mark with upward arrows the galaxy mass bins where a robust Schechter fit could not be achieved. We also carry out a BIC test for all the fits in Fig. 3 to indicate whether a Schechter fit or a power-law fit is more appropriate for the data. The BIC tests for the fits here indicate that a Schechter function is preferred in all cases, except for those that are shown with an upward arrow, where a power-law fit is strongly preferred. It is interesting that in the case where a truncation mass is explicitly included in the model, a fit that does not include one is preferable in some galaxy mass bins. In the 'fiducial' model, both $M_{c,*}$ and CFE scale with birth pressure, therefore where the $M_{c,*}$ is high, also a higher fraction of the mass of the stellar particle is available for GC formation. By contrast in the '$M_{c,*}$ only' model $M_{c,*}$ scales with birth pressure and the CFE does not. As a result, there is less mass available and stellar particles are less likely to form massive GCs. In the 'fiducial' model, high $M_{c,*}$ particles contribute more clusters to the composite cluster mass function than low $M_{c,*}$ particles due to the varying CFE but in the $M_{c,*}$ only model all particles are weighted equally. Therefore when many particles are stacked in the mass function, the power-law index (α) becomes steeper and an $M_{c,*}$ is difficult to identify.

Together, the results in this section confirm that an environmentally varying CFE and mass function truncation, as implemented in the 'fiducial' E-MOSAICS model, is required to explain both the GC and young cluster populations (Pfeffer et al. 2018, 2019; Usher et al. 2018; Reina-Campos et al. 2019; Bastian et al. 2020).

5 DEPENDENCE ON GC DYNAMICAL EVOLUTION

5.1 GC mass loss models

As described in Section 2, the main GC mass loss mechanisms are stellar evolutionary mass loss, tidal shock heating and two-body relaxation. Clusters can be completely removed via dynamical friction. Here we investigate the different mass loss mechanisms and how they affect the GC mass function. We again fit Schechter functions to the GCs in the same galaxy mass bins as in Fig. 1 but we now include two new subsamples of GCs. We include the GCs from the simulations without dynamical friction applied, shown in orange in Figs 4–8, and also the initial GCs that formed with a mass greater than the minimum mass given in Table 1, with no mass loss – stellar or dynamical – applied, shown in green in Figs 4–8. We note that stellar mass loss should affect all GCs approximately equally (assuming the GCs are relatively old) and therefore will not play a part in setting the slope of the GC mass function.

5.1.1 The truncation mass

In Fig. 4, we show the fitted $M_{c,*}$ as a function of galaxy stellar mass, with our fiducial, no dynamical friction (no DF) and no mass loss (initial masses) GC models shown in blue, orange and green, respectively, and the Jordán et al. (2007) fits shown as black stars.

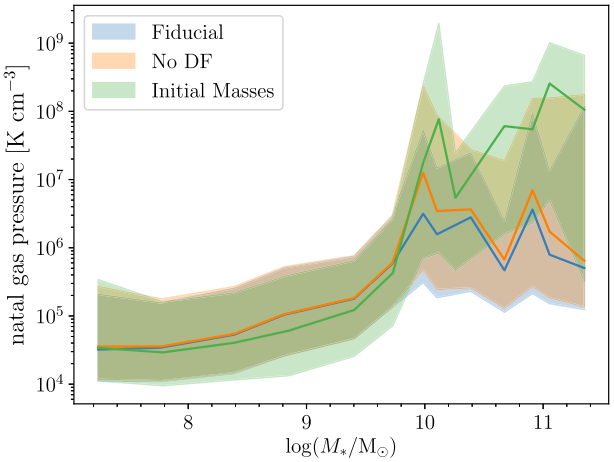

Figure 5. The dependence of GC birth pressure on galaxy stellar mass in the E-MOSAICS galaxy cluster. The shaded regions show the 16th–84th percentile range.

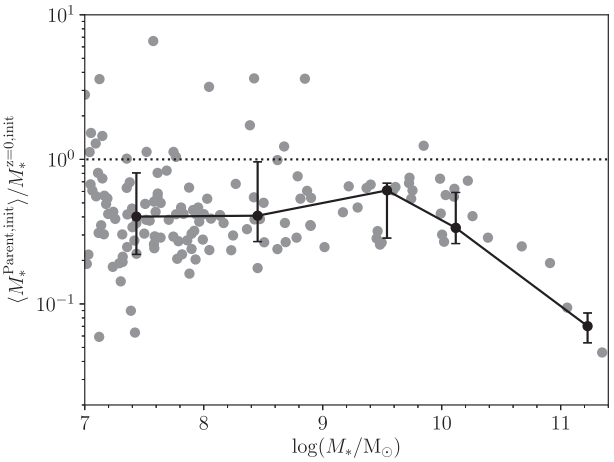

Figure 6. The ratio of the median initial parent galaxy stellar mass to the initial stellar mass of each GC-hosting galaxy in the E-MOSAICS galaxy cluster at $z = 0$. The black points and line show the median and 16th–84th percentile ranges in galaxy mass bins of 1 dex.

Fig. 4 shows that the subsample of GCs that does not include any mass loss (initial masses) has the highest $M_{\rm c,*}$, followed by the subsample that includes all mass-loss mechanisms, except dynamical friction (no DF) and then the fiducial E-MOSAICS model exhibiting the lowest $M_{\rm c,*}$ in a given galaxy mass bin. The $M_{\rm c,*}$ decreases by ∼40 per cent due to stellar evolution, however any further decrease is due to dynamical evolution. This indicates that the GC disruption time-scale is short enough to destroy high mass GCs, and that dynamical evolution plays an important role in shaping the high mass end of the GC mass function.

We relate the galaxy mass to the birth pressure of the GCs in Fig. 5, which shows the birth pressure of the different subsamples of GCs in the same galaxy mass bins as in Fig. 4, where the solid line shows the median and the shaded region represents the 16th–84th percentile range. The birth pressures of the three subsamples are very similar up to a galaxy mass of $\approx 10^{10} M_\odot$, because the samples themselves are similar, i.e. there are not many GCs formed that do not survive until the present day. Above a galaxy mass of $\approx 10^{10} M_\odot$, there is a steep increase in the initial birth pressures before a plateau. It is also at this mass where there is a separation in the median birth pressures between the 'initial masses' sample ($P/k \sim 10^8$ K cm^{-3}) and the other two populations ($P/k \sim 10^6$ K cm^{-3}).

This separation occurs because of the high birth pressures of the initial GCs. In high pressure/high density environments, mass loss mechanisms such as tidal shocks are more prevalent and therefore quickly disrupt the newly formed GCs (termed the 'cruel cradle effect', Kruijssen et al. 2012a; see also Section 6.2 of Pfeffer et al. 2018 in relation to the E-MOSAICS simulations). The tidal disruption timescale is much smaller than the dynamical friction timescale; therefore, before dynamical friction can act, GCs that have formed in the highest pressure environments have already been disrupted. Dynamical friction then becomes effective at reducing $M_{\rm c,*}$ at a galaxy mass of $\approx 10^{10} M_\odot$ but this is not reflected in the birth pressures. This is simply because dynamical friction removes the most massive GCs that are few in number, so although this will affect the $M_{\rm c,*}$ it will not affect the median birth pressures of the surviving GCs.

An interesting feature of Figs 4 and 5 is that both the $M_{\rm c,*}$ of the initial GCs and the natal birth pressure show a plateau above $\log(M_*/M_\odot) \approx 10$ while we might intuitively expect a continuing increase with galaxy mass, with more massive galaxies able to form a greater number of more massive GCs. We must consider, however that massive galaxies grow via mergers and therefore the massive galaxy we observe at $z = 0$ is an accumulation of many galaxy building blocks. Therefore, we must investigate not the galaxy mass at $z = 0$ but rather the galaxy mass at the time of GC formation. For this, we compare the median stellar mass of the galaxies in which the 'initial' GCs formed (the parent galaxy mass) to the $z = 0$ galaxy stellar mass. This is shown in Fig. 6, where each grey point represents one galaxy in the cluster and the black line shows the median for galaxy mass bins of 1 dex. Note that the y-axis shows the ratio of the stellar mass without stellar evolution taken into account, this is to remove the effect of some galaxies having more evolved stellar populations. Fig. 6 shows that the median GC parent galaxy mass relative to the $z = 0$ galaxy mass is broadly constant for $\log(M_*/M_\odot) < 10$, but it declines to higher masses. Above a stellar mass of 10^{10} M$_\odot$ there is a higher fraction of GCs that were born in a lower mass galaxy compared to their host galaxy at $z = 0$. Therefore, the birth pressures and subsequently $M_{\rm c,*}$ remain constant, even with increasing $z = 0$ mass. This is because massive galaxies increasingly grow by mergers, not star formation, so they are unlikely to be forming new GCs during their late accretion-driven growth stage (e.g. Oser et al. 2010; Lee & Yi 2013; Qu et al. 2017; Clauwens et al. 2018; Davison et al. 2020).

Another interesting feature of Fig. 4 is that the effect of dynamical evolution is not constant across all galaxy mass bins. Dynamical mass loss has the most power at reducing $M_{\rm c,*}$ from the initial masses of all GCs to the masses at $z = 0$ at $\log(M_*/M_\odot) \approx 10$. As discussed previously, it is the addition of dynamical friction that drives the decrease in $M_{\rm c,*}$ at these galaxy masses through the removal of the most massive GCs. Here we discuss why this is more efficient at a galaxy mass of $\log(M_*/M_\odot) \approx 10$ than for $\log(M_*/M_\odot) \approx 11$.

The first contributing factor to longer dynamical friction timescales (and therefore a higher chance of survival) is the mass ratio between the GC mass and the galaxy mass. When the mass within the GC's orbit is larger, the dynamical friction timescale is longer ($\tau_{\rm df} \propto V_c$, Lacey & Cole 1993). In the more massive galaxies, the mass within the GC's orbit is likely to be larger at a fixed radius and therefore the GC can survive for longer. The second contributing factor to longer dynamical friction timescales is the radius of the GC orbit. Importantly, GCs may get pushed to wider orbits via mergers (e.g.

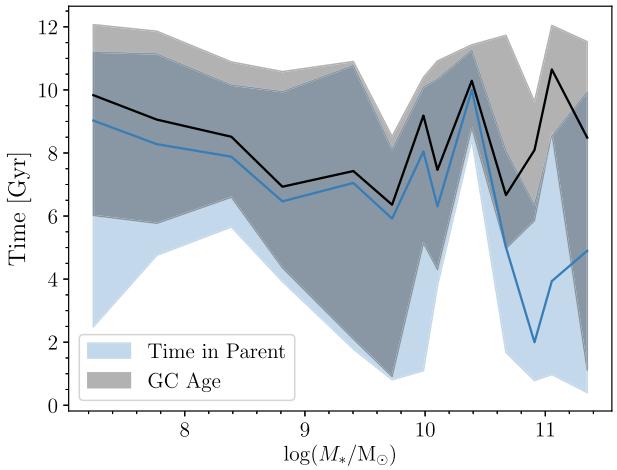

Figure 7. The dependence on the median time a GC spends in its parent galaxy as a function of galaxy stellar mass. The colours of the three subsamples are the same as in Fig. 4 and the shaded regions show the 16th–84th percentile range.

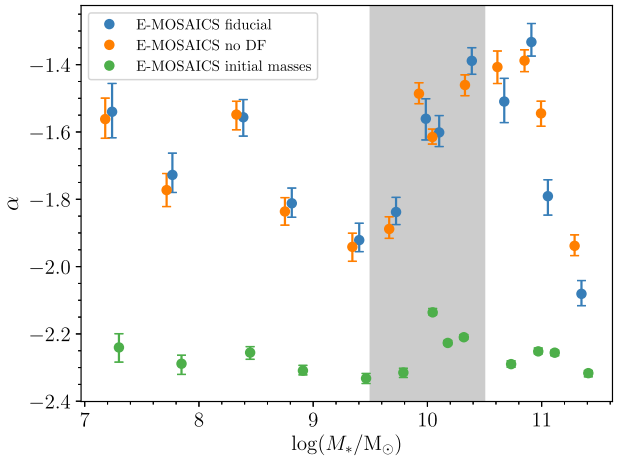

Figure 8. The dependence of α on galaxy stellar mass in the E-MOSAICS galaxy cluster. The blue points show the E-MOSAICS fiducial model at z=0. The orange points show the E-MOSAICS model with no dynamical friction taken into account. Finally, the green points show the E-MOSAICS clusters that survive to z = 0 within our mass cut but with no mass loss (stellar evolution or dynamical) taken into account. The shaded region indicates where the increase of α with galaxy mass is due to increasing cluster mass loss.

Kruijssen et al. 2011). Mergers facilitate the means for GCs to move from their birth places (where dynamical friction timescales may be short) either by being kicked out of the inner parts of the galaxy or being deposited in the halo of a more massive galaxy (where dynamical friction timescales are very long). Qu et al. (2017), along with Clauwens et al. (2018) and Davison et al. (2020), showed that the EAGLE galaxies are built by mainly in-situ star formation up to a stellar mass $\approx 10^{10} M_\odot$. The ex-situ fraction then increases with stellar mass, and for galaxies that reach a stellar mass $\approx 10^{11} M_\odot$ approximately 50 per cent of their mass is built through mergers. Thus, plausibly, it is the lack of redistribution of massive GCs by mergers which leads to more effective dynamical friction in $\sim 10^{10}$ M$_\odot$ galaxies.

To quantify this, we now consider how long the GCs in each $z = 0$ galaxy typically spend in their parent galaxy (i.e. the time between GC formation and $z = 0$ for *in situ* GCs, or the time between formation and the merger of the host galaxy in the case of accreted GCs). This will inform us about whether the GC population is dominated by GCs that have survived in their parent galaxies for a long time or by GCs that have been deposited into the halo of the more massive galaxy after spending a short amount of time in their parent galaxy. We examine this in Fig. 7 where we present the median age and 16th–84th percentile range of the GCs and the median time and 16th–84th percentile range the GCs spent in the parent galaxy (analogous to Fig. D2 in Kruijssen et al. 2019a). The median age of the GCs remains old (> 7 Gyr) at all galaxy masses. Note the slight decline in age with increasing mass from 10^7 towards 10^{10} M$_\odot$, this is because more massive galaxies are likely to have entered the potential well of the galaxy cluster more recently, and, when they do enter the potential well of the galaxy cluster, they can hold on to their star forming gas for longer than their lower mass counter parts (see e.g. Gunn & Gott 1972; Hughes et al. 2019 for more details). The time spent in the parent galaxy traces the age of the GCs closely upto a mass of $\log(M_*/M_\odot) \approx 10.5$ where the time spent in the parent galaxy decreases, whilst the median age still remains old. This reflects the fraction of GCs accreted from satellites into the halo of the galaxy where the dynamical timescale is long and massive GCs can survive.

In conclusion, we suggest that it is the combination of more massive GC formation and then the subsequent mass dependence of the galaxy merger histories and the effect of dynamical friction that leads to the fiducial trend between $M_{c,*}$ and galaxy mass in both the Jordán et al. (2007) work and the E-MOSAICS simulations.

5.1.2 *The mass function slope*

For completeness, we now consider the slope of the mass function in Fig. 8 where we show the power-law index (α) of the Schechter fit in the same galaxy stellar mass bins, where the different coloured points have the same meaning as in Fig. 4. Due to the mass- and environmentally dependent cluster mass-loss mechanisms in the simulations (tidal shocks and two–body relaxation), the recovered power-law indices will depend on the minimum cluster mass for fitting and the strength of cluster mass loss in each galaxy. We note that the minimum GC mass is different in each of these galaxy mass bins (see Table 1) because we are fitting the top two decades of the mass function. Therefore, the power-law index is derived from a different GC mass range in low-mass compared to high-mass galaxies. In particular, the minimum GC mass changes from $\sim 10^3$ to $\sim 10^4$ M$_\odot$ for galaxy masses between $\log(M_*/M_\odot) \approx$ 7-9.5, and from $\sim 10^4$ to $\sim 10^5$ M$_\odot$ for galaxy masses $\log(M_*/M_\odot) \approx$ 10.5–11.5. Thus, some of the variation of α with galaxy mass will be caused by the varying minimum mass.

In Appendix A (lower panel of Fig. A1), we compare power-law indices with different assumptions for the minimum cluster mass in the mass function fits. For masses $\log(M_*/M_\odot) < 9.5$ and >10.5, the power-law indices from the Schechter fits do not depend strongly on the adopted lower mass limit. For masses $9.5 < \log(M_*/M_\odot) < 10.5$ (also highlighted in Fig. 8), there is a strong dependence on α with minimum mass, such that the mass functions are steeper with increasing lower mass limit. α increases with galaxy mass in this mass range, that is, the slope of the power-law portion of the mass function becomes shallower. We can associate this with a rise in the birth pressures with increasing galaxy mass across the same galaxy

mass range (Fig. 5). As discussed above (and in further detail in Pfeffer et al. 2018), a higher birth pressure/density environment [2] leads to effective disruption of GCs and this is particularly prevalent in the low mass GCs, thus leading to a flattening of the mass function. Interestingly, for $M_* > 10^{10.5}\,\mathrm{M}_\odot$ the power-law indices become smaller (steeper mass functions) with increasing galaxy mass, i.e. low-mass cluster mass loss is less effective in the higher mass galaxies, at odds with the observed increasing GC turnover mass with galaxy mass (Jordán et al. 2007; Villegas et al. 2010). This is found for all minimum mass assumptions in Fig. A1. This may be caused by the increasing importance of galaxy mergers with increasing galaxy mass (as discussed in the previous section) resulting in a shorter time for cluster mass loss (Fig. 7) before migration to a less disruptive environment (i.e. regions with weaker tidal fields).

Fig. 8 shows that the GC sample with no mass loss have a relatively consistent power-law index, independently of galaxy mass. E-MOSAICS adopts $\alpha = -2$ for each star particle that forms a GC population. We would therefore expect that the subsample of GCs with no mass loss would have $\alpha = -2$, however Fig. 8 shows a steeper slope for this GC subsample. This is the effect of stacking many star particles (cluster subsamples), each with their own value for $M_{\mathrm{c},*}$; the environmentally-dependent $M_{\mathrm{c},*}$ means that those particles with lower $M_{\mathrm{c},*}$ will contribute relatively more low-mass GCs, steepening the slope of the mass function.

Fig. 8 also shows that dynamical friction does not play a part in shaping the slope of the $z = 0$ mass function, as expected. Dynamical friction time scales grow rapidly towards lower mass GCs as $\tau_{\mathrm{DF}} \propto M_{\mathrm{GC}}^{-1}$ and therefore dynamical friction takes much longer to remove GCs with masses $M < M_{\mathrm{c},*}$. By contrast, tidal shocks and two-body relaxation have a less obvious scaling with galaxy mass, because they depend on many galaxy properties. Therefore, although dynamical processes do shape the slope of the GC mass function, dynamical friction is not one of them.

6 CONCLUSIONS

In this paper, we investigate the origins of the shape of the high-mass end of the GC mass function as a function of galaxy stellar mass in a galaxy cluster. To carry out this analysis, we have used the most massive galaxy group in the E-MOSAICS 34.4^3 cMpc^3 periodic volume. This choice was made to facilitate comparison to the observational results of Jordán et al. (2007) who fit evolved Schechter functions to GCs binned according to host galaxy mass in the Virgo Cluster.

Firstly we examine whether fitting Schechter functions is preferable over fitting power-law functions to the high-mass end of GC mass distributions. This is decided via a BIC test which penalizes a maximum likelihood estimation based on the number of free parameters. We find that for the fiducial physics model in the simulations a Schechter function is preferable and therefore we can confidently compare the truncation mass of the Schechter function in the simulations to those of the observations in Jordán et al. (2007). Fig. 1 shows excellent agreement between the $M_{\mathrm{c},*}$ of the simulations and the observations within the uncertainties.

To further investigate the input physics in the simulations we fit Schechter functions to the GCs that survive to $z = 0$ under three different sets of cluster formation physics that do not allow the CFE, $M_{\mathrm{c},*}$ or both, to vary with environment (Fig. 3). The model that does not let either the CFE or the $M_{\mathrm{c},*}$ vary with environment still prefers a Schechter fit to a power-law fit because of dynamical friction disrupting the most massive GCs. However, this model yields an increasing $M_{\mathrm{c},*}$ with galaxy mass due to a size-of-sample effect, and produces the wrong slope. The model that only allows the CFE to vary with environment again prefers a Schechter fit due to dynamical friction, but $M_{\mathrm{c},*}$ remains too high to match observations. Finally, the model that only allows the $M_{\mathrm{c},*}$ to vary with environment often prefers a power-law fit. This is because the high mass end of the mass function is not well sampled. Therefore it is only the fiducial model with an environmentally-dependent CFE and $M_{\mathrm{c},*}$ that matches both the absolute values and the shape of the $M_{\mathrm{c},*}$ trend with galaxy stellar mass. This adds to the body of work already supporting the initial physics and subsequent evolution of star clusters in the E-MOSAICS simulations. We therefore conclude that we can use the E-MOSAICS simulations to investigate the origin and shape of the observed trend.

Jordán et al. (2007) consider the argument that the decrease of $M_{\mathrm{c},*}$ with decreasing galaxy mass could be due to the stronger depletion of massive GCs in dwarf galaxies due to dynamical friction. They postulate this because the dynamical friction timescale is proportional to the galaxy's circular speed ($\tau_{DF} \propto V_{\mathrm{c}}$) implying that the relevance of dynamical friction can increase in lower mass galaxies. They then rule out this hypothesis concluding that dynamical friction can only account for a small fraction of the steepening (decreasing $M_{\mathrm{c},*}$) of the mass function with time. In the E-MOSAICS simulations, dynamical friction is applied in post-processing and therefore we can easily disable its effects and we do so in Fig. 4 and 8. In the high-mass end of the GC mass function (Fig. 4) we do not find that dynamical friction becomes more important in the lower-mass galaxies. In fact dynamical friction has a very small effect in these galaxies and the effect of dynamical friction on the slope of the GC mass function is negligible across all galaxy masses (Fig. 8). Therefore our findings support the Jordán et al. (2007) claim that dynamical friction does not play an important role at low galaxy masses. However, at a galaxy stellar mass $\approx 10^{10}\,\mathrm{M}_\odot$ dynamical friction and other mass loss mechanisms are important in setting the shape of the high-mass end of the GC mass function (Fig. 4).

GCs are formed with increasing $M_{\mathrm{c},*}$ with galaxy mass until a galaxy mass $\log(M_*/M_\odot) \approx 10$ where $M_{\mathrm{c},*}$ reaches a plateau and remains constant up to the largest masses. This is because the birth pressure also plateaus at these galaxy masses. The birth pressure plateaus because massive galaxies grow primarily by late mergers, and their GCs form in lower mass progenitors which have correspondingly lower pressures than the present day descendant.

Although $M_{\mathrm{c},*}$ follows this trend at birth it is how the GCs are then nurtured by their parent galaxy that sets the final $M_{\mathrm{c},*}$ we can observe today. This depends on whether the galaxy is able to move its high-mass GCs out of their highly disruptive birth environments quickly enough for them to survive until the present day. Galaxies can redistribute their GCs when they undergo merger events. Up until a stellar mass of $10^{10}\,\mathrm{M}_\odot$ galaxies are built by mainly *in-situ* star formation and therefore do not undergo enough mergers to re-distribute their GCs, leading to the destruction of their massive GCs. This means that disruption of all kinds is most efficient at reducing $M_{\mathrm{c},*}$ at a stellar mass of around $10^{10}\,\mathrm{M}_\odot$ where the pressures/densities are high enough to form and then subsequently destroy high-mass GCs and there is not enough merger activity to redistribute them.

In conclusion, we find that it is a combination of both nature and nurture that sets the $z = 0\,M_{\mathrm{c},*}$ trend with galaxy mass. It is in

[2]Though density is the most relevant quantity when considering cluster mass loss, birth density and pressure are directly proportional (thus can be interchanged in analysis) due to the imposed equation of state at high gas densities in the EAGLE model.

the galaxy's nature to form more massive GCs if the galaxy itself is massive, but these GCs must be nurtured and redistributed via mergers if they are to survive until $z = 0$.

ACKNOWLEDGEMENTS

JP and NB gratefully acknowledge funding from the ERC under the European Union's Horizon 2020 research and innovation programme via the ERC Consolidator Grant Multi-Pop (grant agreement number 646928). JP gratefully acknowledges financial support from the Australian Research Council's Discovery Projects funding scheme (DP200102574). JMDK gratefully acknowledges funding from the Deutsche Forschungsgemeinschaft (DFG, German Research Foundation) through an Emmy Noether Research Group (grant number KR4801/1-1). JMDK and STG gratefully acknowledge funding from the European Research Council (ERC) under the European Union's Horizon 2020 research and innovation programme via the ERC Starting Grant MUSTANG (grant agreement number 714907). RAC is a Royal Society University Research Fellow. MRC gratefully acknowledges the Canadian Institute for Theoretical Astrophysics (CITA) National Fellowship for partial support. This study made use of high-performance computing facilities at Liverpool John Moores University, partly funded by the Royal Society and LJMUs Faculty of Engineering and Technology. This work used the DiRAC Data Centric system at Durham University, operated by the Institute for Computational Cosmology on behalf of the STFC DiRAC HPC Facility (www.dirac.ac.uk). This equipment was funded by BIS National E-infrastructure capital grant ST/K00042X/1, STFC capital grants ST/H008519/1 and ST/K00087X/1, STFC DiRAC Operations grant ST/K003267/1 and Durham University. DiRAC is part of the National E-Infrastructure.

DATA AVAILABILITY

The data underlying this article will be shared on reasonable request to the corresponding author.

REFERENCES

Adamo A. et al., 2017, ApJ, 841, 131
Adamo A. et al., 2020, Space Sci. Rev., 216, 69
Adamo A., Bastian N., 2018, in Stahler S., ed., The Lifecycle of Clusters in Galaxies. Vol. 424, Astrophysics and Space Science Library, Springer International Publishing, Cham, p. 91
Adamo A., Kruijssen J. M. D., Bastian N., Silva-Villa E., Ryon J., 2015, MNRAS, 452, 246
Bastian N., Konstantopoulos I. S., Trancho G., Weisz D. R., Larsen S. S., Fouesneau M., Kaschinski C. B., Gieles M., 2012, A&A, 541, A25
Bastian N., Pfeffer J., Kruijssen J. M. D., Crain R. A., Trujillo-Gomez S., Reina-Campos M., 2020, MNRAS, 498, 1050
Baumgardt H., 1998, A&A, 330, 480
Baumgardt H., Parmentier G., Anders P., Grebel E. K., 2013, MNRAS, 430, 676
Bik A., Lamers H. J. G. L. M., Bastian N., Panagia N., Romaniello M., 2003, A&A, 397, 473
Booth C. M., Schaye J., 2009, MNRAS, 398, 53
Brodie J. P., Strader J., 2006, ARA&A, 44, 193
Burkert A., Smith G. H., 2000, ApJ, 542, L95
Chandar R. et al., 2010, ApJ, 719, 966
Chandar R., Whitmore B. C., Calzetti D., O'Connell R., 2014, ApJ, 787, 17
Chandar R., Whitmore B. C., Dinino D., Kennicutt R. C., Chien L. H., Schinnerer E., Meidt S., 2016, ApJ, 824, 71
Chevance M. et al., 2020, Space Sci. Rev., 216, 50
Clauwens B., Schaye J., Franx M., Bower R. G., 2018, MNRAS, 478, 3994
Côté P. et al., 2004, ApJS, 153, 223
Crain R. A. et al., 2015, MNRAS, 450, 1937
Crain R. A. et al., 2017, MNRAS, 464, 4204
Dalla Vecchia C., Schaye J., 2012, MNRAS, 426, 140
Davison T. A., Norris M. A., Pfeffer J. L., Davies J. J., Crain R. A., 2020, MNRAS, 497, 81
de Grijs R., Bastian N., Lamers H. J. G. L. M., 2003, ApJ, 583, L17
Dowell J. D., Buckalew B. A., Tan J. C., 2008, AJ, 135, 823
Drinkwater M. J., Gregg M. D., Colless M., 2001, ApJ, 548, L139
Durrell P. R., Harris W. E., Geisler D., Pudritz R. E., 1996, AJ, 112, 972
Elmegreen B. G., 2010, ApJ, 712, L184
Elmegreen B. G., 2011, in Charbonnel C., Montmerle T., eds, EAS Publications Series. Vol. 51, EAS Publications Series, p. 31
Fall S. M., Zhang Q., 2001, ApJ, 561, 751
Fonnesbeck C., Patil A., Huard D., Salvatier J., 2015, PyMC: Bayesian Stochastic Modelling in Python. Astrophysics Source Code Library, record ascl:1506.005
Forbes D. A. et al., 2018, Proc. R Soc. London Ser. A, 474, 20170616
Furlong M. et al., 2015, MNRAS, 450, 4486
Furlong M. et al., 2017, MNRAS, 465, 722
Gieles M., Zwart S. F. P., Baumgardt H., Athanassoula E., Lamers H. J. G. L. M., Sipior M., Leenaarts J., 2006a, MNRAS, 371, 793
Gieles M., Larsen S. S., Bastian N., Stein I. T., 2006b, A&A, 450, 129
Goudfrooij P., 2004, in Lamers H. J. G. L. M., Smith L. J., Nota A., eds, Astronomical Society of the Pacific Conference Series Vol. 322, The Formation and Evolution of Massive Young Star Clusters. p. 469
Gunn J. E., Gott J. Richard I., 1972, ApJ, 176, 1
Hanes D. A., 1977, MNRAS, 180, 309
Harris W. E., 2001, in Labhardt L., Binggeli B., eds, Saas-Fee Advanced Course 28: Star Clusters. Springer-Verlag, Berlin, p. 223
Harris W. E., Pudritz R. E., 1994, ApJ, 429, 177
Harris W. E., Racine R., 1979, ARA&A, 17, 241
Hughes M. E., Pfeffer J., Martig M., Bastian N., Crain R. A., Kruijssen J. M. D., Reina-Campos M., 2019, MNRAS, 482, 2795
Hughes M. E., Pfeffer J. L., Martig M., Reina-Campos M., Bastian N., Crain R. A., Kruijssen J. M. D., 2020, MNRAS, 491, 4012
Johnson L. C. et al., 2017, ApJ, 839, 78
Jordán A. et al., 2007, ApJS, 171, 101
Kashibadze O. G., Karachentsev I. D., Karachentseva V. E., 2020, A&A, 635, A135
Keller B. W., Kruijssen J. M. D., Pfeffer J., Reina-Campos M., Bastian N., Trujillo-Gomez S., Hughes M. E., Crain R. A., 2020, MNRAS, 495, 4248
Kissler-Patig M., Richtler T., Hilker M., 1996, A&A, 308, 704
Kruijssen J. M. D. et al., 2020, MNRAS, 498, 2472
Kruijssen J. M. D., 2012, MNRAS, 426, 3008
Kruijssen J. M. D., 2014, Classical and Quantum Gravity, 31, 244006
Kruijssen J. M. D., Pelupessy F. I., Lamers H. J. G. L. M., Portegies Zwart S. F., Icke V., 2011, MNRAS, 414, 1339
Kruijssen J. M. D., Maschberger T., Moeckel N., Clarke C. J., Bastian N., Bonnell I. A., 2012a, MNRAS, 419, 841
Kruijssen J. M. D., Pelupessy F. I., Lamers H. J. G. L. M., Portegies Zwart S. F., Bastian N., Icke V., 2012b, MNRAS, 421, 1927
Kruijssen J. M. D., Pfeffer J. L., Crain R. A., Bastian N., 2019a, MNRAS, 486, 3134
Kruijssen J. M. D., Pfeffer J. L., Reina-Campos M., Crain R. A., Bastian N., 2019b, MNRAS, 486, 3180
Krumholz M. R., McKee C. F., Bland-Hawthorn J., 2019, ARA&A, 57, 227
Lacey C., Cole S., 1993, MNRAS, 262, 627
Lagos C. d. P. et al., 2015, MNRAS, 452, 3815
Larsen S. S., 2002, AJ, 124, 1393
Larsen S. S., 2009, A&A, 494, 539
Lee J., Yi S. K., 2013, ApJ, 766, 38
Liu Y., Peng E. W., Jordán A., Blakeslee J. P., Côté P., Ferrarese L., Puzia T. H., 2019, ApJ, 875, 156
Mackey A. D. et al., 2019, MNRAS, 484, 1756
McCrady N., Graham J. R., 2007, ApJ, 663, 844
McLaughlin D. E., 1999, ApJ, 512, L9
Messa M. et al., 2018a, MNRAS, 473, 996

Messa M. et al., 2018b, MNRAS, 477, 1683
Miller B. W., Whitmore B. C., Schweizer F., Fall S. M., 1997, AJ, 114, 2381
Mok A., Chandar R., Fall S. M., 2019, ApJ, 872, 93
Okazaki T., Tosa M., 1995, MNRAS, 274, 48
Oser L., Ostriker J. P., Naab T., Johansson P. H., Burkert A., 2010, ApJ, 725, 2312
Peng E. W. et al., 2008, ApJ, 681, 197
Pfeffer J., Kruijssen J. M. D., Crain R. A., Bastian N., 2018, MNRAS, 475, 4309
Pfeffer J., Bastian N., Kruijssen J. M. D., Reina-Campos M., Crain R. A., Usher C., 2019, MNRAS, 490, 1714
Portegies Zwart S. F., McMillan S. L. W., Gieles M., 2010, ARA&A, 48, 431
Qu Y. et al., 2017, MNRAS, 464, 1659
Racine R., 1980, in Hesser J. E., ed., Star Clusters. Vol. 85, Proc. IAU Symp., p. 369
Reina-Campos M., Kruijssen J. M. D., 2017, MNRAS, 469, 1282
Reina-Campos M., Kruijssen J. M. D., Pfeffer J., Bastian N., Crain R. A., 2018, MNRAS, 481, 2851
Reina-Campos M., Kruijssen J. M. D., Pfeffer J. L., Bastian N., Crain R. A., 2019, MNRAS, 486, 5838
Reina-Campos M., Hughes M. E., Kruijssen J. M. D., Pfeffer J. L., Bastian N., Crain R. A., Koch A., Grebel E. K., 2020, MNRAS, 493, 3422
Rosas-Guevara Y. M. et al., 2015, MNRAS, 454, 1038
Schaye J. et al., 2015, MNRAS, 446, 521
Schaye J., Dalla Vecchia C., 2008, MNRAS, 383, 1210
Schechter P., 1976, ApJ, 203, 297
Schwarz G., 1978, Annals of Statistics, 6, 461
Surdin V. G., 1979, Soviet Ast., 23, 648
Toomre A., 1964, ApJ, 139, 1217
Trayford J. W. et al., 2015, MNRAS, 452, 2879
Trujillo-Gomez S., Kruijssen J. M. D., Reina-Campos M., Pfeffer J. L., Keller B. W., Crain R. A., Bastian N., Hughes M. E., 2021, MNRAS, 503, 31
Usher C., Pfeffer J., Bastian N., Kruijssen J. M. D., Crain R. A., Reina-Campos M., 2018, MNRAS, 480, 3279
van den Bergh S., 1985, ApJ, 297, 361
Vesperini E., 1998, MNRAS, 299, 1019
Vesperini E., Zepf S. E., Kundu A., Ashman K. M., 2003, ApJ, 593, 760
Villegas D. et al., 2010, ApJ, 717, 603
Whitmore B. C., Schweizer F., 1995, AJ, 109, 960
Whitmore B. C., Zhang Q., Leitherer C., Fall S. M., Schweizer F., Miller B. W., 1999, AJ, 118, 1551
Whitmore B. C., Chandar R., Bowers A. S., Larsen S., Lindsay K., Ansari A., Evans J., 2014, AJ, 147, 78
Wiersma R. P. C., Schaye J., Theuns T., Dalla Vecchia C., Tornatore L., 2009, MNRAS, 399, 574
Zhang Q., Fall S. M., 1999, ApJ, 527, L81

APPENDIX A: THE FITTING RESULTS UNDER VARYING ASSUMPTIONS

The Schechter fits described in this work use a varying minimum mass which depends on the maximum GC mass in a particular galaxy mass bin. Jordán et al. (2007) also have a GC completeness luminosity that scales approximately with galaxy mass. In lower mass galaxies, lower mass GCs are more readily observable, due to the lower surface brightness of the galaxy. We choose a minimum GC mass to be 2 dex below the third most massive GC (to account for stochasticity at the high-mass end) but we now show the effect of using a constant minimum mass on the $M_{\mathrm{c},*}$.

In the upper panel of Fig. A1 we compare the results of Schechter fits with varying minimum mass limits. The choice of minimum mass does somewhat affect the output of the Schechter fit (generally resulting in a slightly larger $M_{\mathrm{c},*}$ with larger minimum mass), but the trend of $M_{\mathrm{c},*}$ with M_* remains similar. However, if the limit is too large then the window of masses we are fitting for some galaxies is too small for a robust fit. This is clear for the mass limit of $10^5\,\mathrm{M}_\odot$ in the galaxies with $\log(M_*/\mathrm{M}_\odot) < 9.5$. In many of these cases a Schechter fit could not be found and if one was outputted, the $M_{\mathrm{c},*}$ was greater than the maximum GC mass (shown by open symbols).

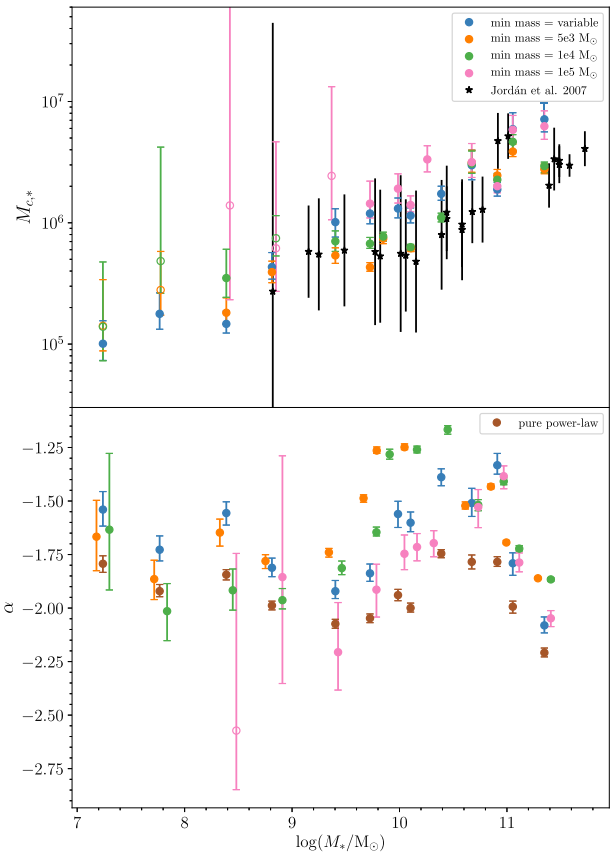

Figure A1. $M_{\mathrm{c},*}$ and α as a function of galaxy mass for four different minimum mass cases. The variable case uses the minimum masses shown in table 1. The open symbols represent cases where the $M_{\mathrm{c},*}$ from the Schechter fit is larger than the maximum GC mass in the galaxy bin. These are cases where a robust Schechter fit has not been found. In the lower panel we also show the slope obtained when fitting a pure power-law model, which is obtained by using a varying minimum mass.

In the lower panel of Fig. A1 we present the value of the power-law index under these varying minimum mass assumptions. For galaxy masses $M_* \lesssim 10^{9.5}\,\mathrm{M}_\odot$ the power-law indices obtained are relatively similar for all minimum mass assumptions, with the except for the $> 10^5\,\mathrm{M}_\odot$ limit which results in too few GCs for a robust fit at low galaxy masses. For galaxies with $M_* > 10^{9.5}\,\mathrm{M}_\odot$ the power-law indices depend strongly on the lower mass limit (even though the recovered $M_{\mathrm{c},*}$ is relatively insensitive). This indicate cluster mass loss is more important for these simulated galaxies, resulting in flatter mass functions at lower masses. The indices obtained for a pure power-law fit are generally steeper than for Schechter models, which is expected given a single power-law function must also account for the steeper upper truncation of the mass functions.

This paper has been typeset from a TEX/LATEX file prepared by the author.